Journal of Applied Mathematics and Physics (ZAMP)
Vol. 39, March 1988

0044-2275/88/002186-18 $ 5.10/0


# Mixed convection on a vertical circular cylinder

By T. Mahmood and J. H. Merkin, Dept. of Applied Mathematical Studies, University of Leeds, Leeds LS2 9JT, Great Britain

## 1. Introduction

The problem of the mixed convection boundary-layer flow on a vertical plate has been discussed in some detail, by, amongst others [1, 2, 3, 4, 5]. The problem of the mixed convection on a horizontal cylinder has been treated by Merkin [6]. The occurrence of dual solutions in mixed convection similarity solutions was shown by Wilks and Bramley [7], they also considered the eigenvalue problem arising out of a linear stability analysis of these solutions.

However, the problem of mixed convection in axi-symmetric boundary layers has received much less attention, and, perhaps, the easiest of such problems to set up is the boundary-layer flow over a vertical circular cylinder, held at a constant temperature in a uniform free stream $U_0$. Previously Narain and Uberoi [8], have considered the problem of the combined forced and free-convection heat transfer thin needles in a uniform external stream, obtaining a series and local similarity solutions. The related problem with a prescribed wall heat flux has been treated by Mucoglu and Chen [9], they gave results only for moderate distances from the leading edge.

Glauert and Lighthill [10], have investigated the forced flow problem, giving two methods for obtaining a solution. One is a Pohlhausen method, based on a velocity profile chosen to represent conditions near the surface as accurately as possible. The other is asymptotic series solution, valid far enough downstream from the leading edge for the boundary-layer thickness to have become large compared with the cylinder radius. This asymptotic series was also given by Stewartson [11]. For this problem Seban and Bond [12], obtained a series solution valid near the leading edge where the boundary layer is thin compared to the cylinder radius.

We show that in the mixed convection problem the flow depends on the buoyancy parameter $\alpha = \dfrac{Gr}{Re}$. When $\alpha > 0$ when the buoyancy forces act in the same direction as the flow and so aid the development of the boundary layer, whereas when $\alpha < 0$ they oppose its development.

We obtain a solution for the present problem by first deriving a series solution for small $X$ (where $X$ measures (non-dimensional) distance from the leading edge). The leading order term is the Blasius flat plate solution and we find that the curvature effects give an $0(X^{1/2})$ perturbation to this, while the contribution from the buoyancy force first appears at $0(X)$. This series solution is then extended by a numerical solution of the full boundary-layer equations. We find that for $\alpha > 0$ this numerical solution can give accurate results only up to moderate values of $X$ as, for large $X$, the solution develops a logarithmic singularity on the cylinder. Then, following [10], we obtain an approximate solution valid for all $X$; we find that this solution gives a good approximation for small $X$. For large $X$ we find that the flow is essentially free convection, the asymptotic solution of this problem has been given by Kuiken [13], and on comparing with his solution we find that our approximate solution has the correct asymptotic behaviour.

For $\alpha < 0$ the boundary layer separates at a finite value $X_s$ of $X$ with a flow reversal indicated. We find for moderate values of $\alpha$, at least, that near $X = X_s$ the solution behaves in a regular way, without the singularity that was reported for the flat plate problem [1].

## 2. Equations of motion

Consider a uniform stream $U_0$ flowing past a fixed vertical cylinder of radius $a$. The temperature of the cylinder is held at the constant value $T_1$ different to that of the ambient fluid which has temperature $T_0$.

The boundary-layer equations governing the flow are:

$$\frac{\partial}{\partial x}(r u) + \frac{\partial}{\partial r}(r w) = 0 \tag{1}$$

$$u\frac{\partial u}{\partial x} + w\frac{\partial u}{\partial r} = g\beta(T - T_0) + \nu\left(\frac{\partial^2 u}{\partial r^2} + \frac{1}{r}\frac{\partial u}{\partial r}\right) \tag{2}$$

$$u\frac{\partial T}{\partial x} + w\frac{\partial T}{\partial r} = \kappa\left(\frac{\partial^2 T}{\partial r^2} + \frac{1}{r}\frac{\partial T}{\partial r}\right) \tag{3}$$

together with the boundary conditions

$$\left.\begin{aligned} &u = w = 0, \quad T = T_1 \quad \text{on} \quad r = a \\ &u \to U_0, \quad T \to T_0 \quad \text{as} \quad r \to \infty \end{aligned}\right\} \tag{4}$$

where $u, w$ are velocity components in the $x, r$ directions, $\beta$ is the coefficient of thermal expansion, $g$ is acceleration due to gravity, $\nu$ and $\kappa$ are the kinematic viscosity and the thermal diffusivity respectively. Equations (1)–(3) can be made

non-dimensional by introducing the non-dimensional variables,

$$R = r/a, \quad X = (x/a)\, Re^{-1}, \quad U = \frac{u}{U_0}, \quad W = \frac{w}{U_0} Re, \quad \theta = \frac{T - T_0}{\Delta T} \tag{5}$$

where $Re$ is the Reynolds number given by $Re = \dfrac{U_0 a}{\nu}$ and $\Delta T = T_1 - T_0$. In (5) the transverse coordinate $r$ is made non-dimensional using the cylinder radius $a$, whereas the much longer scale $aRe$ ($Re \gg 1$) is used for the streamwise coordinate $x$. This, in turn, implies that, as in [10, 11, 13], the present discussion is for thin cylinders, i.e. cylinders which are long compared with their radius.

Using (5), Eqs. (1)–(3) become

$$\frac{\partial}{\partial X}(RU) + \frac{\partial}{\partial R}(RW) = 0 \tag{6}$$

$$U\frac{\partial U}{\partial X} + W\frac{\partial U}{\partial R} = \alpha\theta + \frac{\partial^2 U}{\partial R^2} + \frac{1}{R}\frac{\partial U}{\partial R} \tag{7}$$

$$U\frac{\partial \theta}{\partial X} + W\frac{\partial \theta}{\partial R} = \frac{1}{Pr}\left(\frac{\partial^2 \theta}{\partial R^2} + \frac{1}{R}\frac{\partial \theta}{\partial R}\right) \tag{8}$$

where $Pr$ is the Prandtl number and $\alpha = \dfrac{g\beta\Delta T a^2}{U_0 \nu} = Gr/Re$ is the buoyancy parameter; $\alpha > 0$ for aiding flows (i.e. where the buoyancy force acts in the same direction as the flow) and $\alpha < 0$ for opposing flows (i.e. where the buoyancy force and the flow are in opposite directions). The boundary conditions are

$$\left.\begin{aligned} &U = W = 0, \quad \theta = 1 \quad \text{on} \quad R = 1 \\ &U \to 1, \quad \theta \to 0 \quad \text{as} \quad R \to \infty \end{aligned}\right\} \tag{9}$$

## 3. Solution

### *(a) Series solution for X small*

Near the leading edge the flow will be basically that on a flat plate, with the effects of the curvature of the cylinder and the buoyancy forces having only small effects. This suggests the transformation

$$\psi = X^{1/2} f(X, \eta), \quad \theta = \theta(X, \eta), \quad \eta = \frac{R^2 - 1}{2X^{1/2}} \tag{10}$$

where $\psi$ is the stream function defined so that

$$U = \frac{1}{R}\frac{\partial \psi}{\partial R}, \quad W = -\frac{1}{R}\frac{\partial \psi}{\partial X}.$$

Substituting (10) into Eqs. (7) and (8) gives

$$(1 + 2\eta X^{1/2})\frac{\partial^3 f}{\partial \eta^3} + 2X^{1/2}\frac{\partial^2 f}{\partial \eta^2} + \alpha\theta X + \tfrac{1}{2} f\frac{\partial^2 f}{\partial \eta^2} = X\left(\frac{\partial f}{\partial \eta}\frac{\partial^2 f}{\partial \eta\,\partial X} - \frac{\partial f}{\partial X}\frac{\partial^2 f}{\partial \eta^2}\right) \tag{11}$$

$$(1 + 2\eta X^{1/2})\frac{\partial^2 \theta}{\partial \eta^2} + 2X^{1/2}\frac{\partial \theta}{\partial \eta} + \tfrac{1}{2} Pr\, f\frac{\partial \theta}{\partial \eta} = X\,Pr\left(\frac{\partial f}{\partial \eta}\frac{\partial \theta}{\partial X} - \frac{\partial f}{\partial X}\frac{\partial \theta}{\partial \eta}\right) \tag{12}$$

with boundary conditions

$$\left.\begin{aligned} &f = 0, \quad \frac{\partial f}{\partial \eta} = 0 \text{ on } \eta = 0, \quad \frac{\partial f}{\partial \eta} \to 1 \text{ as } \eta \to \infty \\ &\theta = 1 \text{ on } \eta = 0, \quad \theta \to 0 \text{ as } \eta \to \infty \end{aligned}\right\}. \tag{13}$$

Equations (11) and (12) suggest an expansion for $f(X, \eta)$ and $\theta(X, \eta)$ for small $X$ in the form

$$\left.\begin{aligned} f(X, \eta) &= f_0(\eta) + X^{1/2} f_1(\eta) + X f_2(\eta) + \cdots \\ \theta(X, \eta) &= \theta_0(\eta) + X^{1/2}\theta_1(\eta) + X\theta_2(\eta) + \cdots \end{aligned}\right\}. \tag{14}$$

We can see from Eqs. (11) and (12) that curvature effects appear in the $0(X^{1/2})$ terms, while the buoyancy force effects first appear at $0(X)$. This requires us to split up $f_2$ and $\theta_2$ as $f_2 = F_2 + \alpha\varphi_2$ and $\theta_2 = \bar{\theta}_2 + \alpha h_2$, where the equations for $F_2$ and $\bar{\theta}_2$ include just the curvature effects, and $\varphi_2$ and $h_2$ include just the buoyancy effects. The resulting equations have to be solved numerically. To do this we used the known numerical solution of the leading order term in Eq. (11), (the Blasius equation) which has $f_0''(0) = 0.33206$ and for $Pr = 1$, $\theta_0'(0) = -0.33206$. This gave for $Pr = 1$, $f_1''(0) = 0.69432$, $f_2''(0) = -0.65658 + 1.14666\,\alpha$, $\theta_1'(0) = -0.69432$, $\theta_2'(0) = 0.65658 - 0.27108\,\alpha$.

Using these values it follows that the non-dimensional skin friction coefficient $Cf = \left(\frac{1}{R}\frac{\partial U}{\partial R}\right)_{R=1} = \frac{1}{X^{1/2}}\left(\frac{\partial^2 f}{\partial \eta^2}\right)_{\eta=0}$ is given by:

$$Cf = X^{-1/2}(0.33206 + 0.69432\,X^{1/2} + (-0.65658 + 1.14666\,\alpha)X + \cdots) \tag{15}$$

and that Nusselt number

$$Nu = -\left(\frac{1}{R}\frac{\partial \theta}{\partial R}\right)_{R=1} = -\frac{1}{X^{1/2}}\left(\frac{\partial \theta}{\partial \eta}\right)_{\eta=0} \text{ is given by,}$$

$$Nu = X^{-1/2}(0.33206 + 0.69432\,X^{1/2} - (0.65658 - 0.27108\,\alpha)X + \cdots). \tag{16}$$

*(b) Finite-difference solution*

Because near the leading edge the flow is basically that on a flat plate, with the effects of the curvature of the cylinder and the buoyancy forces having only small effects, transformed Eqs. (11) and (12) are the appropriate ones to solve numerically starting at the leading edge. However to remove the singularity in these equations at $X = 0$ arising from the $X^{1/2}$ term we first put $\xi = X^{1/2}$, giving the equations, for $Pr = 1$,

$$(1 + 2\eta\xi)\frac{\partial^3 f}{\partial\eta^3} + 2\xi\frac{\partial^2 f}{\partial\eta^2} + \alpha\xi^2\theta + \tfrac{1}{2}f\frac{\partial^2 f}{\partial\eta^2}$$

$$= \xi/2\left(\frac{\partial f}{\partial\eta}\frac{\partial^2 f}{\partial\eta\,\partial\xi} - \frac{\partial f}{\partial\xi}\frac{\partial^2 f}{\partial\eta^2}\right) \tag{17}$$

$$(1 + 2\eta\xi)\frac{\partial^2\theta}{\partial\eta^2} + 2\xi\frac{\partial\theta}{\partial\eta} + \tfrac{1}{2}f\frac{\partial\theta}{\partial\eta} = \xi/2\left(\frac{\partial f}{\partial\eta}\frac{\partial\theta}{\partial\xi} - \frac{\partial f}{\partial\xi}\frac{\partial\theta}{\partial\eta}\right). \tag{18}$$

To solve Eqs. (17) and (18) numerically we use $q = \dfrac{\partial f}{\partial\eta}$ and $\theta$ as dependent variables, and then replace the derivatives in $\xi$-direction by differences and all other quantities by averages. On writing $v = v_1 + v_2$, $u = \theta_1 + \theta_2$ and $\lambda = \dfrac{\xi_1 + \xi_2}{\Delta\xi}$, Eqs. (17) and (18) become

$$[1 + \eta(\xi_1 + \xi_2)]\frac{d^2 v}{d\eta^2} + \left[(\xi_1 + \xi_2) + \int_0^\eta \left\{\left(\frac{1}{4} + \frac{\lambda}{4}\right)v - \frac{1}{2}\lambda q_1\right\} d\eta\right]\frac{dv}{d\eta}$$

$$+ \alpha u\left(\frac{\xi_1 + \xi_2}{2}\right)^2 - \frac{1}{4}\lambda v(v - 2q_1) = 0 \tag{19}$$

$$[1 + \eta(\xi_1 + \xi_2)]\frac{d^2 u}{d\eta^2} + \left[(\xi_1 + \xi_2) + \int_0^\eta \left\{\left(\frac{1}{4} + \frac{\lambda}{4}\right)v - \frac{1}{2}\lambda q_1\right\} d\eta\right]\frac{du}{d\eta}$$

$$- \frac{1}{4}\lambda v(u - 2\theta_1) = 0. \tag{20}$$

The derivatives in the $\eta$-direction are then replaced by central differences, giving finally the system of nonlinear algebraic equations:

$$v_{j+1} - 2v_j + v_{j-1} + \frac{h^2}{2[1 + jh(\xi_1 + \xi_2)]}(v_{j+1} - v_{j-1}) \cdot \left[\frac{\xi_1 + \xi_2}{h} + \left(\frac{1}{4} + \frac{\lambda}{4}\right) V_j - \frac{1}{2}\lambda\delta_j\right] + \alpha\left(\frac{\xi_1 + \xi_2}{2}\right)^2 \frac{h^2}{[1 + jh(\xi_1 + \xi_2)]} u_j - \frac{\lambda h^2}{4[1 + jh(\xi_1 + \xi_2)]}(v_j^2 - 2q_{1j}v_j) = 0 \tag{21}$$

$$u_{j+1} - 2u_j + u_{j-1} + \frac{h^2}{2[1 + jh(\xi_1 + \xi_2)]}(u_{j+1} - u_{j-1}) \cdot \left[\frac{\xi_1 + \xi_2}{h} + \left(\frac{1}{4} + \frac{\lambda}{4}\right) V_j - \frac{1}{2}\lambda\delta_j\right] - \frac{\lambda h^2}{4[1 + jh(\xi_1 + \xi_2)]} v_j(u_j - 2\theta_{1j}) = 0 \tag{22}$$

($j = 1, 2, 3 \ldots n$). Where $h$ is the step length in the $\eta$-direction and where

$$V_j = (v_1 + v_2 + \cdots + \tfrac{1}{2}v_j) \text{ and } \delta_j = (q_1 + q_2 + \cdots + \tfrac{1}{2}q_j).$$

These nonlinear algebraic equations are solved iteratively using the Newton-Raphson method. Starting with initial estimates for $v_j$ and $u_j$ (the values calculated at the previous step) a new value for $v_j$ was obtained using Eq. (21). Then using these values for $v_j$ in Eq. (22), a better estimate for $u_j$ was calculated. The process was continued until the difference between successive iterates in both $v_j$ and $u_j$ was less than $10^{-6}$. The process was found to converge easily, usually taking no more than 4 iterations to achieve convergence.

To start the integration at $\xi = 0$ values of $f_0'$ and $\theta_0$ obtained from expansion (14) were used. The integration then proceeded for increasing $\xi$ in step-by-step manner. To maintain accuracy in the $\xi$-direction the step from $\xi$ to $\xi + \Delta\xi$ was covered in first one and then two steps with the step-length $\Delta\xi$ being adjusted so as to keep the differences between these two solutions less than $5.10^{-5}$. At each step, the values of $q$ and $\theta$ obtained via the two-step integration were used. Having calculated the velocity and temperature profiles the skin friction parameter $Cf = \frac{1}{\xi}\left(\frac{\partial q}{\partial \eta}\right)_{\eta=0}$ and Nusselt number $Nu = -\frac{1}{\xi}\left(\frac{\partial \theta}{\partial \eta}\right)_{\eta=0}$ were calculated at each step in the $\xi$-direction.

*(c) Approximate method*

To obtain an approximate solution, which is valid for all $X$, we use an integrated form of the energy Eq. (8), namely

$$\frac{d}{dX}\left(\int_1^\infty RU\theta\,dR\right) = -\frac{1}{Pr}\left(\frac{\partial\theta}{\partial R}\right)_{R=1} \tag{23}$$

and take approximate forms for the temperature and velocity profiles as

$$\left.\begin{aligned} &\theta = 1 - \frac{1}{A}\log R \\ &U = \frac{\alpha}{4}(1-R^2) + \frac{1}{A}\left(1 + \frac{\alpha}{4}(e^{2A}-1)\right)\log R \\ &\theta = 0, \quad U = 0, \quad R > e^A. \end{aligned}\right\} 1 < R < e^A \tag{24}$$

These profiles are chosen so as to satisfy the conditions that

$$\theta = 1, \quad U = 0 \text{ on } R = 1; \quad \theta \to 0, \quad U = 1 \text{ as } R \to \infty. \tag{25}$$

The form for the temperature profile is suggested by the approximate solution for the flow past a cylinder derived by Glauert and Lighthill, [10], while the form for the velocity profile arises from the condition, from Eq. (7), that for $R \cong 1$, $\frac{\partial}{\partial R}\left(R\frac{\partial U}{\partial R}\right) \cong -\alpha R$. Integrating this twice, and using (25) gives the expression for $U$ in (24). Substituting (24) into Eq. (23) gives an ordinary differential equation for $A$ which, for $Pr = 1$, is

$$\begin{aligned} \frac{dA}{dX} = \Bigg[&\left(\frac{3\alpha}{16} - \frac{19\alpha}{64A} + \frac{\alpha}{8A^2}\right)e^{4A} \\ &+ \left(\frac{1}{2} + \frac{\alpha}{8} - \frac{3}{4A} + \frac{3\alpha}{16A} + \frac{1}{2A^2} - \frac{\alpha}{4A^2}\right)e^{2A} \\ &- \frac{1}{4A} + \frac{\alpha}{16A} + \frac{3\alpha}{64A} - \frac{1}{2A^2} + \frac{\alpha}{8A^2}\Bigg]^{-1}. \end{aligned} \tag{26}$$

Equation (26) can be solved implicitly for $X$ in terms of $A$ subject to $X = 0$ at $A = 0$ to give

$$\begin{aligned} X = &\frac{3\alpha}{64}e^{4A} + \frac{1}{4}\left(1 + \frac{\alpha}{4}\right)e^{2A} + \frac{1}{8A}(4(1-e^{2A}) - \alpha(1 + e^{4A} - 2e^{2A})) \\ &+ \frac{13\alpha}{64}\int_0^A \left(\frac{e^{4S}-1}{S}\right)dS + \left(\frac{1}{4} - \frac{11\alpha}{16}\right)\int_0^A \left(\frac{e^{2S}-1}{S}\right)dS. \end{aligned} \tag{27}$$

For small $X$, (27) gives $A \cong (12\,X)^{1/2}$, independent of $\alpha$, from which it follows that

$$Nu = 0.289\,X^{-1/2}. \tag{28}$$

This is seen to be in good agreement with the correct form for $Q$ near $X = 0$ as given by (16). For $X$ large and $\alpha > 0$, $X \cong \frac{3\alpha}{64} e^{4A}$, so that

$$Nu \sim \frac{4}{\log\left(\frac{64\,X}{3\alpha}\right)} \tag{29}$$

for $X \gg 1$.

## 4. Results

*(a) Aiding case, $\alpha > 0$*

Consider first the case when $\alpha > 0$ (i.e. where the buoyancy forces act in the same direction as the flow). The effect that the buoyancy forces have on the flow and heat transfer characteristics are shown in Figs. (1a) and (1b) in which the values of $\left(\frac{\partial q}{\partial \eta}\right)_{\eta=0} = Cf\,\frac{Re_x^{1/2}}{Re}$ and $-\left(\frac{\partial \theta}{\partial \eta}\right) = Nu\,\frac{Re_x^{1/2}}{Re}$ respectively, as obtained from the numerical solution described above, have been plotted against $X$ for

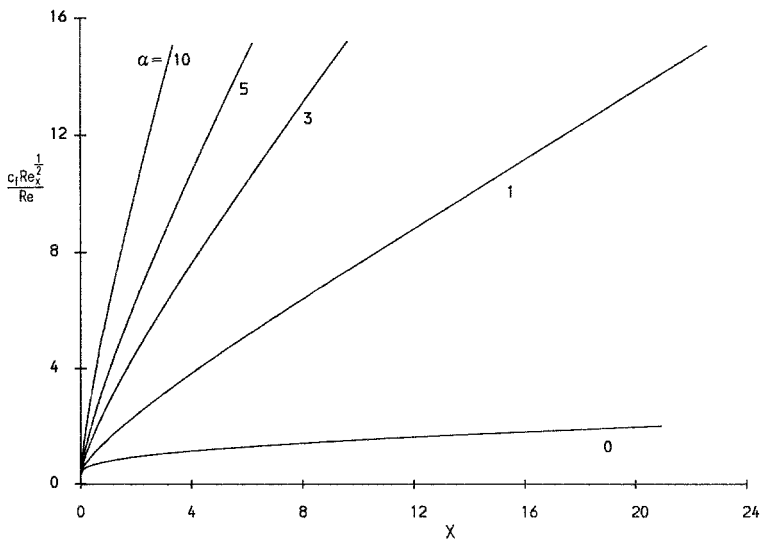


Figure 1a
Graphs of wall velocity gradients $\left(\frac{\partial q}{\partial \eta}\right)_0 = \frac{Re_x^{1/2}}{Re}\,Cf$ plotted against $X$ for various values of $\alpha$ (aiding case).

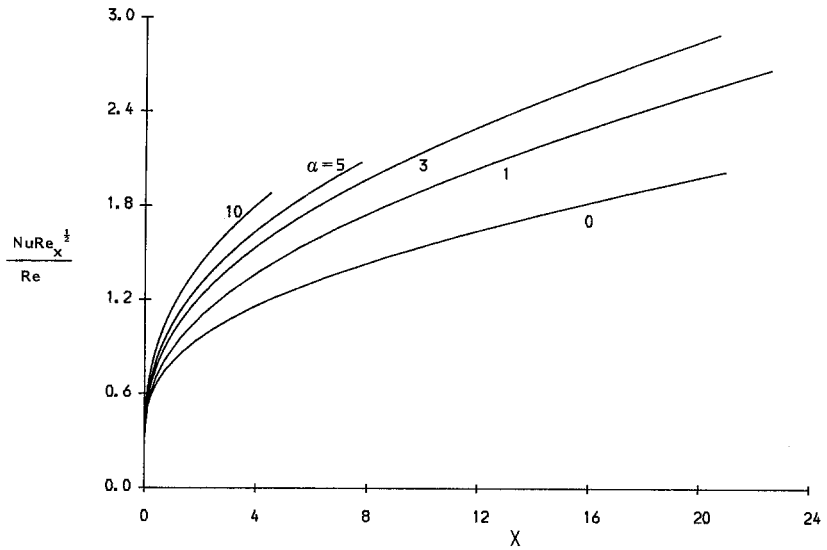


Figure 1b
Graphs of wall temperature gradients $-\left(\frac{\partial\theta}{\partial\eta}\right)_0 = Nu\frac{Re_x^{1/2}}{Re}$ plotted against $X$ for various values of $\alpha$ (aiding case).

various values of $\alpha$. It is evident from these figures that for a given value of $\alpha$, there is rapid increase in these quantities as $X$ increases along the cylinder, with this increase being more pronounced for the larger values of $\alpha$.

The effect that the buoyancy forces have on the flow can also be seen in Figs. (2a) and (2b) in which the graphs of velocity and temperature profiles $\frac{\partial f}{\partial\eta}$ and $\theta$ respectively are plotted against $\eta$ for various values of $X$ for the case when $\alpha = 1$. From Fig. (2a) we can see that close to the leading edge the velocity profile approaches the free stream value from below. Further along the cylinder, where the buoyancy forces have had more opportunity to accelerate the fluid near the cylinder, a velocity "overshoot" results, with the size of this overshoot increasing as $X$ is increased. Also this figure shows that the boundary layer thickness increases considerably away from the leading edge. The effect on the temperature is also appreciable as can be seen from Fig. (2b). The temperature profile shown for $X = 87.4$ is quite different to that at $X = 0$. This has a pronounced double structure, with an initial sharp descrease, followed by a long "tail".

The shapes that the velocity and temperature profiles take as $X$ is increased causes a difficulty for the numerical solution. To account accurately for the rapid change near the cylinder requires a small step length $h$ in the $\eta$-direction, while the long tail requires the outer boundary conditions being applied at successively larger values of $\eta$. This conflict between the need for a small step length and a large range of integration and the need to keep the computation time within reasonable bounds limits the usefulness of the numerical scheme to moderate values of $X$. The same difficulty has been encountered in a similar problem [14].

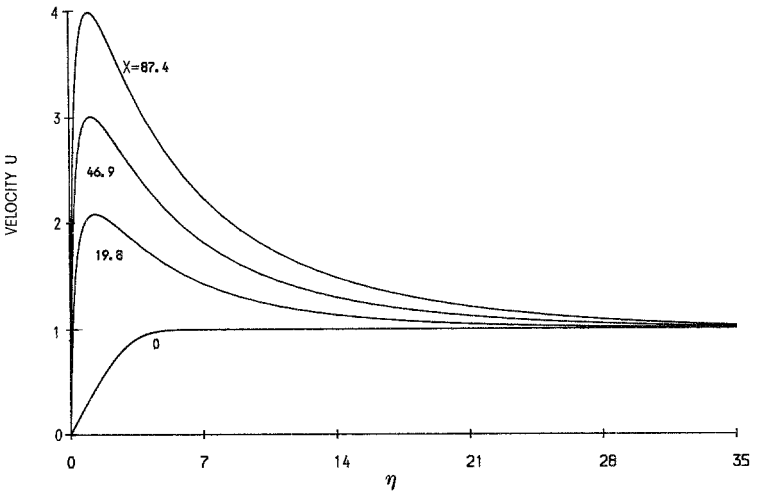


Figure 2a
Velocity profiles at various values of $X$ for $\alpha = 1$.

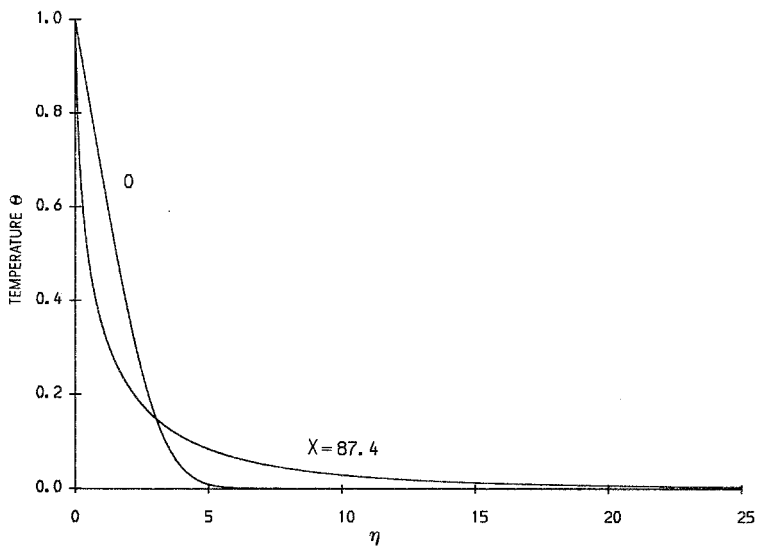


Figure 2b
Temperature profiles at $X = 0$ and $X = 87.4$ for $\alpha = 1$.

Also, as we shall show below, the asymptotic solution for large $X$ is attained only when $\log(X/\alpha) \gg 1$, with this asymptotic solution giving rise to a logarithmic singularity on the cylinder. This renders the use of transformed equations based on the asymptotic solution unsuitable for numerical integration. Consequently the approximate solution is useful in giving estimates for heat transfer (and skin friction) over the full range of $X$ needed.

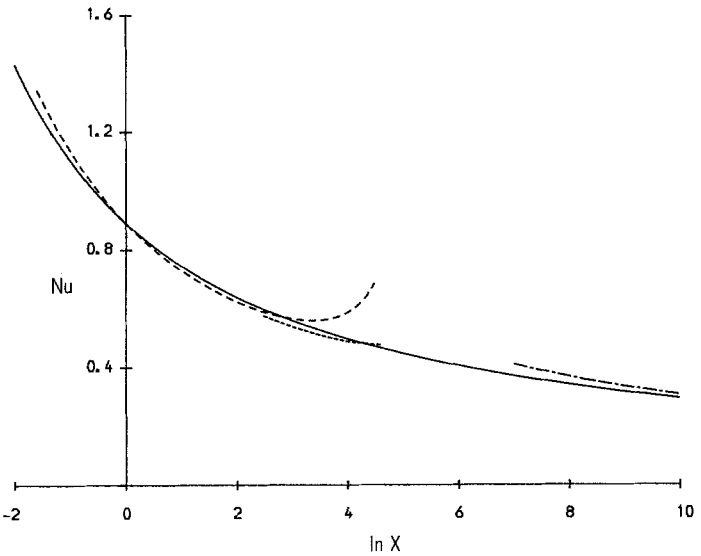


Figure 3
Nusselt number $Nu$, evaluated by the approximate method, plotted against $\log_e X$ (shown by the full line). Graphs of $Nu$ obtained from the numerical solution for $h = 0.1$ (shown by – – –) and $h = 0.05$ (shown by - - - - -) and $Nu$ as given by the asymptotic solution, (39), (shown by – · – · – · –).

In Fig. (3), a graph of $Nu$ against $\log_e X$ is given for $\alpha = 1$ as obtained from (27). Also in this figure are plotted graphs of $Nu$ obtained from the numerical solution (again for $\alpha = 1$), using values of $h = 0.1$ and $h = 0.05$. From these it is apparent that the numerical solution with $h = 0.1$ becomes inaccurate at about $\log_e X = 3 (X \cong 20)$ while the solution with $h = 0.05$ continues to remain accurate beyond this point, before finally becoming inaccurate at about $\log_e X \cong 5 (X \cong 150)$. In both cases the outer boundary conditions were applied at $\eta = 40$.

Both from the numerical and approximate solutions we can see that in the aiding case free convection eventually becomes the main mechanism of heat transfer from the cylinder, with forced convection having an increasingly less significant effect. This is in line with other mixed convection studies for plates [1, 2], but is in contrast to the mixed convection flow past a circular cylinder in a saturated porous medium [15], where at large distances along the cylinder it was forced convection which again became the most important effect.

To obtain the solution for $X \gg 1$, we follow the solution derived by Kuiken [13], for the free convection boundary layer on a vertical cylinder. To do this we first put

$$X = \alpha \bar{X}, \quad U = \alpha \bar{U} \tag{30}$$

so that from (5), $\bar{X}$ and $\bar{U}$ are independent of the free stream $U_0$, with now $x = a\,Gr\,\bar{X}$ and $u = \dfrac{\nu\,Gr\,\bar{U}}{a}$. We then put

$$\psi = \bar{X}\,F(\xi, \bar{X}), \quad \theta = \frac{H(\zeta, \bar{X})}{\log g(\bar{X})}, \quad \zeta = \frac{R^2}{g(\bar{X})}. \tag{31}$$

When (30) and (31) are substituted into Eqs. (7) and (8) and the functions $F(\zeta, \bar{X})$ and $H(\zeta, \bar{X})$ expanded in powers of $(\log g)^{-1}$ we find that, at leading order, $F$ and $G$ satisfy the ordinary differential equations

$$2\zeta H'' + (F+2)H' = 0 \tag{32}$$

$$2\zeta F''' + (2+F)F'' - \tfrac{1}{2}F'^2 + H = 0 \tag{33}$$

(primes denote differentiation with respect to $\zeta$ provided $g(\bar{X})$ satisfies $\dfrac{g^2}{\log g} = 4\bar{X}$, from which it follows that

$$g(\bar{X}) = (2\bar{X}\log 2\bar{X})^{1/2}\left(1 + 0\left(\frac{\log|\log\bar{X}|}{\log\bar{X}}\right)\right). \tag{34}$$

The boundary conditions are that

$$F' \to 0, \quad H \to 0 \quad \text{as} \quad \zeta \to \infty \tag{35}$$

and on the cylinder

$$F = F' = 0, \quad H = 1 \quad \text{on} \quad \zeta g = 1. \tag{36}$$

Using (31) and (34), it follows that the free stream gives a contribution of $0\left(\left(\dfrac{\log\bar{X}}{X}\right)^{1/2}\right)$ which is negligible relative to the expansion variable $(\log g)^{-1}$ and so the effect of the free stream will not be felt in this expansion. From Eq. (32) it follows that, for small $\zeta$

$$H = A_0 \log\zeta + B_0 + \cdots \tag{37}$$

and satisfying (36) gives $A_0 = -1$. Also we require the solution of (33) not to be singular at $\zeta = 0$, so that

$$F \cong C_0\zeta + \cdots. \tag{38}$$

The solution of Eqs. (32) and (33) satisfying (37) and (38) then gives the values of $B_0$ and $C_0$ as $B_0 = 0.231$, $C_0 = 1.436$ for $Pr = 1$ (the results given in [13] were for $Pr = 0.7$). The solution can then proceed to higher order terms. From this solution it follows that

$$Nu \sim \frac{4}{\log(2\bar{X}\log 2\bar{X})} \tag{39}$$

and comparing this with (29) we can see that the approximate solution estimates the heat transfer correctly to leading order. This can be seen from Fig. (3), where values of $Nu$ obtained from (39) are also shown. It is also apparent from the form for large $X$ of the solution given by (37) why transformation (31) required to obtain the asymptotic solution is unsuitable for using in a numerical scheme.

*(b) Opposing case, $\alpha < 0$*

For opposing flows, i.e. $\alpha < 0$, the buoyancy force and the flow are in opposite direction. In Figs. 4(a), (b), (c) and (d), the graphs of wall velocity and

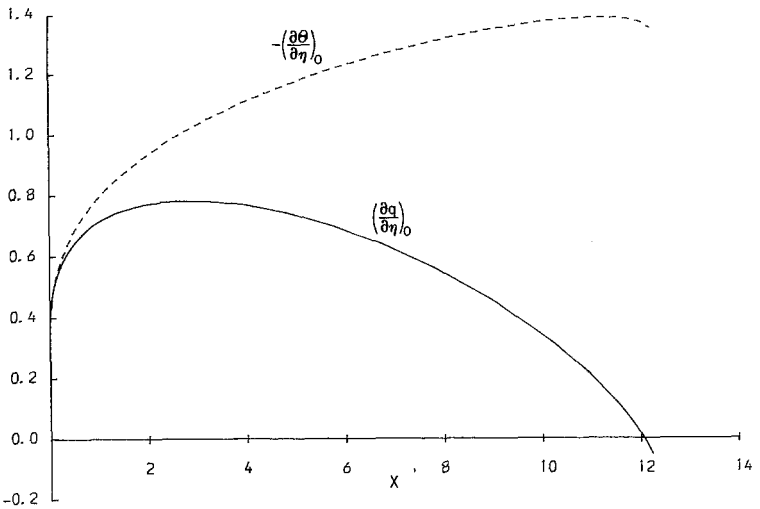


Figure 4
Graphs of wall velocity gradient and temperature gradient (shown by broken line) plotted against $X$ for the opposing case.
Figure 4a. $\alpha = -0.1$.

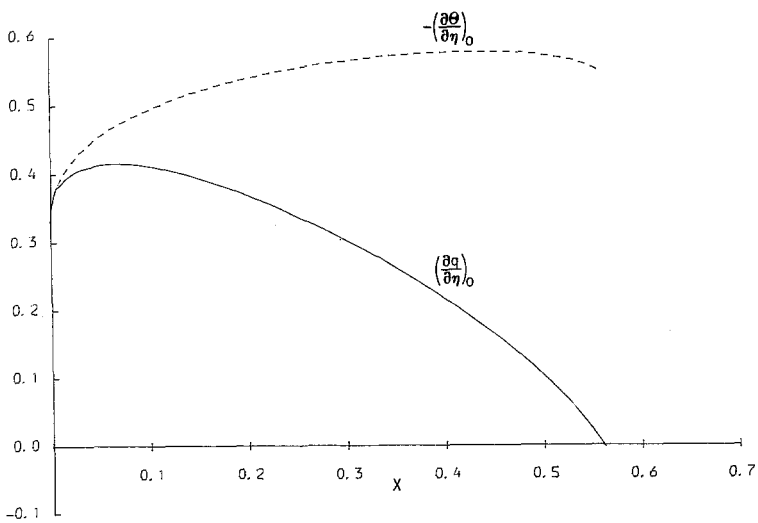


Figure 4b. $\alpha = -1$.

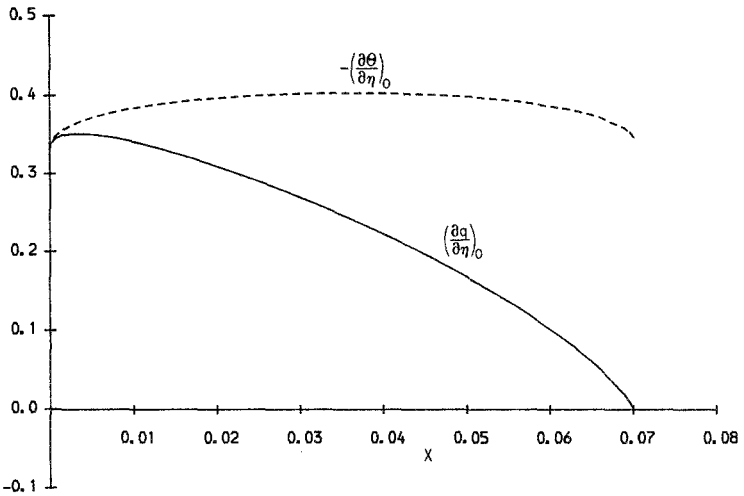


Figure 4c. $\alpha = -5$.

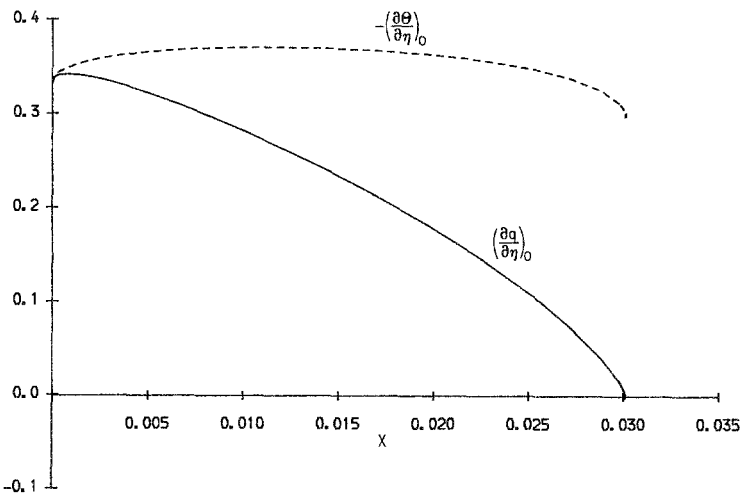


Figure 4d. $\alpha = -10$.

temperature gradients $\left(\frac{\partial q}{\partial \eta}\right)_0$ and $-\left(\frac{\partial \theta}{\partial \eta}\right)_0$ are plotted against $X$ for various values of $\alpha$. These figures indicate that Nusselt number $Nu = -\frac{1}{X^{1/2}}\left(\frac{\partial \theta}{\partial \eta}\right)_0$ decreases slowly while the skin friction goes to zero at a finite value of $X$, $X_s$ (say).

A graph of the values of $X_s$ as obtained from the numerical solution for various values of $\alpha$ is shown in Fig. (6). Also shown in this figure is a graph of $X_s$, as calculated from the series expansion (15). To derive this we

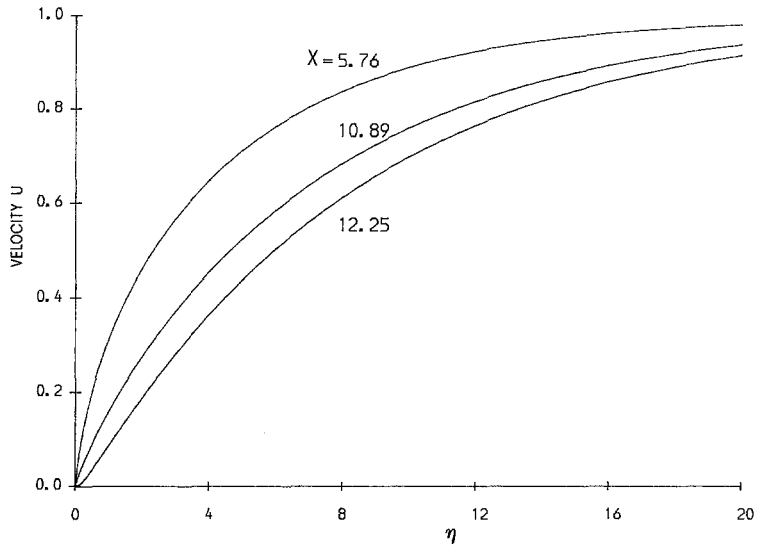


Figure 5a
Velocity profiles at $X = 5.76$, $X = 10.89$ and $X = 12.25$ for $\alpha = -0.1$.

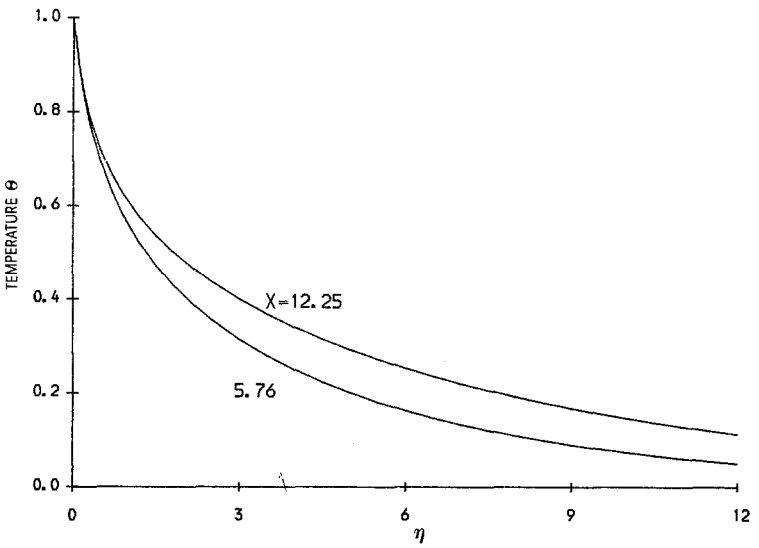


Figure 5b
Temperature profiles at $X = 5.76$ and $X = 12.25$ for $\alpha = -0.1$.

put $Cf = 0$ at $X = X_s$ and solved the resulting quadratic equation for $X_s^{1/2}$ to get, for $Pr = 1$,

$$X_s^{1/2} = [0.529 + (0.280 + 0.506\,(1 + 1.746\,|\alpha|))^{1/2}]/(1 + 1.746\,|\alpha|). \qquad (40)$$

We can see from Fig. (6) that the values of $X_s$ as given by (40) are in good agreement with the numerically determined values at least for the larger values of $\alpha$. Also, we have from (40) that $X_s \sim 0.290/|\alpha|$ for $|\alpha| \gg 1$. For $|\alpha| \gg 1$ the

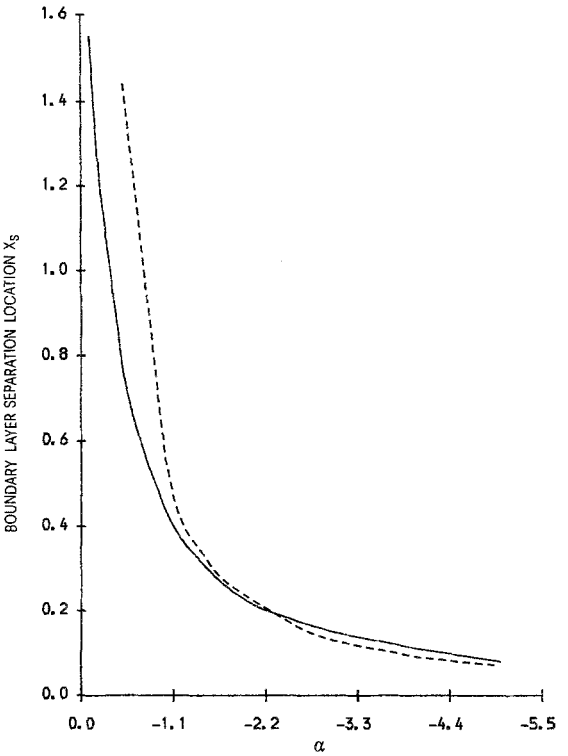


Figure 6
Separation point $X_s$ obtained from the numerical solution (shown by full line), and obtained from (40) (broken line).

effects of curvature will have only a small effect and the flow upto separation will be given basically by the plate solution, [1], from which we can deduce that $|\alpha| X_s \cong 0.192$ for $|\alpha| \gg 1$.

Figures 4(a) and 4(b) show that, for the smaller values of $|\alpha|$, $Cf$ approaches $X_s$ in a regular way, without the appearance of a singularity, as was reported in the plate problem, [1]. With $|\alpha|$ small the curvature of the cylinder has a significant effect on the flow and the numerical solutions suggest that this has the effect of inhibiting the square root singularity near separation that arises in two-dimensional boundary-layer flows, with the solution being regular at separation (or having such a weak singularity which is not picked up by the numerical scheme). In fact the numerical solution for $\alpha = -0.1$ and $\alpha = -1.0$ continued past $X_s$ into a region of reversed flow, where, as expected, it became unstable and broke down.

Velocity and temperature profiles for $\alpha = -0.1$ are shown in Figs. 5a and 5b respectively. These show that the profiles near separation are dominated by curvature effects as can be seen from the two-layer flow pattern, with rapid changes near the wall and a long "tail" region before the outer boundary conditions are attained. In this respect these profiles are similar to those shown in Figs. 2 for the aiding case (though there is no velocity overshoot). The profiles (not given) for the larger values of $|\alpha|$ ($\alpha = -5$ and $\alpha = -10$) do not show the

effects of curvature to any marked degree and are similar to the velocity and temperature profiles for the flat plate problem.

The numerical solution for $\alpha = -0.1$ was continued well past $X_s$ without loss of stability by using the FLARE approximation, [19], (in effect putting the terms $U\frac{\partial U}{\partial X}$ and $U\frac{\partial \theta}{\partial X}$ in Eqs. (7) and (8) to zero wherever $U < 0$). Strictly this method is the first step in an iterative procedure for calculating flows with reversed flow regions. In the model discussed here there is no mechanism for reattachment downstream of separation and so this approach was not pursued further. To proceed in this direction in an attempt to understand the regular behaviour near separation a modification to the model is required. This is, at present, under consideration.

The possibility of a regular solution at separation in mixed convection cannot be disregarded as was shown by Stewartson [16]. (This analysis was for a compressible boundary layer, but the details are the same for mixed convection). The modification of the Goldstein expansion, [17], derived by Buckmaster, [18], to reatain the singularity was required because the numerical solutions indicated strongly that the solution did become singular at separation. For the larger values of $|\alpha|$, the effects of curvature become less important and the plate problem is approached. This can be seen in Fig. 4(c) and particularly in Fig. 4(d) where a singularity in the skin friction at $X = X_s$ is seen. In all cases the heat transfer was non-zero at $X = X_s$.

## Acknowledgement

One of us (T. M.) whishes to thank the Government of Pakistan for the grant to undertake this research.

### References

[1] J. H. Merkin, *The effect of buoyancy forces on the boundary-layer flow over a semi-infinite vertical flat plate in a uniform free stream.* J. Fluid Mech. *35,* 439–450 (1969).

[2] G. Wilks, *The flow of a uniform stream over a semi-infinite vertical flat plate with uniform surface heat flux.* Int. J. Heat Mass Transfer *17,* 743–753 (1974).

[3] R. Hunt and G. Wilks, *On the behaviour of the laminar boundary-layer equations of mixed convection near a point of zero skin friction.* J. Fluid Mech. *101,* 377–391 (1980).

[4] J. Gryzagoridus, *Combined free and forced convection from an isothermal vertical plate.* Int. J. Heat Mass Transfer *18,* 911–916 (1975).

[5] V. P. Carey and B. Gebhart, *Transport at a large downstream distance in mixed convection flow adjacent to a vertical flux surface.* Int. J. Heat Mass Transfer *25,* 255–266 (1982).

[6] J. H. Merkin, *Mixed convection from a horizontal circular cylinder.* Int. J. Heat Mass Transfer *20,* 73–77 (1977).

[7] G. Wilks and J. S. Bramley, *Dual solutions in mixed convection.* Proc. Royal Soc. Edinburgh *87A,* 349–358 (1980).

[8] J. P. Narain and M. S. Uberoi, *Combined forced and free-convection heat transfer from vertical thin needles in a uniform stream.* Phys. Fluids *15,* 1879–1882 (1972).

[9] A. Mucoglu and T. S. Chen, *Buoyancy effects on forced convection along a vertical cylinder with uniform surface heat flux.* J. Heat Transfer, 523–525 (1976).
[10] M. B. Glauert and M. J. Lighthill, *The axisymmetric boundary layer on a long thin cylinder. Proc. Royal Soc.* London *A230,* 188–203 (1955).
[11] K. Stewartson, *The asymptotic boundary layer on a circular cylinder in axial incompressible flow.* Quart. Applied Math. *13,* 113–122 (1955).
[12] R. A. Seban and R. Bond, *Skin friction and heat transfer characteristics of a laminar boundary layer on a cylinder in axial incompressible flow.* J. Aero. Sci. *18,* 671–675 (1951).
[13] H. K. Kuiken, *The thick free-convection boundary-layer along a semi-infinite isothermal vertical cylinder.* J. Applied Maths & Physics (ZAMP) *25,* 497–514 (1974).
[14] J. H. Merkin, *Free convection from a vertical cylinder embedded in a saturated porous medium.* Acta Mech. *62,* 19–28 (1986).
[15] J. H. Merkin and I. Pop, *Mixed convection boundary layer on a vertical cylinder embedded in a saturated porous medium.* Acta Mech. *66* 251–262 (1987).
[16] K. Stewartson, *The behaviour of a laminar compressible boundary layer near a point of zero skin friction.* J. Fluid Mech. *12,* 117–128 (1962).
[17] S. Goldstein, *On laminar boundary layer flow near a position of separation.* Quart. J. Mech. & Applied Maths. *1,* 43–69 (1948).
[18] J. Buckmaster, *The behaviour of a laminar compressible boundary layer on a cold wall near a point of zero skin friction.* J. Fluid Mech. *44,* 237–247 (1970).
[19] T. A. Reyhner and I. Flügge-Lotz, *The interaction of a shock wave with a laminar boundary layer.* Int. J. Non-linear Mech. *3,* 173–199 (1968).

**Abstract**

The problem of the mixed convection boundary-layer flow past an isothermal vertical circular cylinder is considered in both the cases when the buoyancy forces aid and oppose the development of the boundary layer. A series solution is obtained, valid near the leading edge, and this is extended by a numerical solution of the full equations, which in the aiding case, becomes inaccurate downstream. An approximate solution is also derived which gives a good estimate for the heat transfer near the leading edge and has the correct asymptotic form well downstream. In the opposing case, the boundary layer is seen to separate at a finite distance downstream, with, for moderate values of the buoyancy parameter, the numerical solution indicating a regular behaviour near separation.

(Received: February 10, 1987; revised: October 13, 1987)